RSC Mechanochemistry

ROYAL SOCIETY OF CHEMISTRY

PAPER

View Article Online
View Journal

Cite this: DOI: 10.1039/d6mr00009f

Why are zeolites harder to make than MOFs? A study of the sodalite system

Haochen Wu, [a] Daniel N. Rainer, [b] Simon J. Coles, [b] Samuel J. Page[c] and Stuart L. James *[a]

The mechanochemical synthesis of zeolites is far less developed than that of MOFs, despite the need for more sustainable production of these commodity materials. Grinding (potentially involving mechanochemistry) followed by heating has been investigated but in many cases the individual roles of these activation methods have not been elucidated. Also, reactants that might corrode steel vessels (*e.g.* NaOH), have often been used. Here, we systematically investigate the mechanochemical synthesis of sodalite (SOD) to elucidate the key factors. To aid diffusion and minimise reaction times we have investigated liquid Si sources (tetraethoxysilane, TEOS; vinyltriethoxysilane VTEOS; and phenyltriethoxysilane, PTEOS) in reaction with NaOH and $Al(OAc)_2OH$. With TEOS, ball milling without heating gave a quantitative reaction (by ^{27}Al MAS NMR) in as little as 50 min, but only amorphous phases were formed (as shown by PXRD). Organosilanes enabled solvent-free synthesis of organic-functionalised SOD phases. Acetate-impregnated phases, *e.g.* $[Al_3Si_3O_{12}]_2[Na_4OAc]_2$, were obtained arising from the use of $Al(OAc)_2OH$ as Al source. 3D Electron Diffraction (3DED) was used to characterise TSOD and VSOD giving $a = 9.0311(7)$ for TSOD and 9.0718(9) for VSOD. The larger cell of the latter is consistent with the accommodation of vinyl groups. Use of $Na_2SiO_3{\cdot}5H_2O$ as Si source to avoid NaOH, in closed steel vessels with short heating periods at moderate temperatures (*e.g.*, 0.5–4 h at 100–300 °C) gave the acetate-impregnated SOD phase $[Al_3Si_3O_{12}]_2[Na_4OAc]_2$ in high crystallinity (up to 94%) and with N_2-BET surface areas similar to the highest literature values from hydrothermal synthesis (*e.g.* 44.7 $m^2\ g^{-1}$). Overall, we note that milling the reactants prior to heating often gave no clear advantage compared to simple hand-mixing prior to heating. Notably, heating was always required to crystallise the product into the zeolite structure. We ascribe this to the high Si–O and Al–O bond strengths which necessitate heating to cause recrystallisation into ordered phases in contrast to MOFs based on more labile bonds. This study has clarified some of the technical challenges and factors to consider in mechanochemical zeolite synthesis and presents an efficient method for solventless SOD synthesis in closed vessels. The potential for developing continuous zeolite synthesis by twin-screw extrusion (TSE) is also discussed.

Received 24th January 2026
Accepted 10th April 2026

DOI: 10.1039/d6mr00009f

rsc.li/RSCMechanochem

Introduction

Zeolites are microporous crystalline materials composed of TO_4 (T = Si, Al, Ti, Sn, *etc.*) tetrahedra with oxygen atoms connecting adjacent tetrahedra.[1] They are produced on very large scales (~1.7–2.0 million metric tons per year[2]) for a wide range of applications. However, the conventional hydrothermal synthetic method most widely used has poor sustainability on account of its low efficiency (*e.g.* large amounts of solvent, long reaction times and low reactor capacity) and in many cases use of sacrificial (and costly) organic structure directing agents (OSDAs). The search for cheaper, faster and more sustainable synthetic methods is therefore important. Solventless, template-free routes would be particularly advantageous.[3] Correspondingly, there have been many studies on solventless zeolite synthesis which have been reviewed.[4,5] Materials such as Zeolite Socony Mobil-5 (ZSM-5, MFI),[6] Linde Type A zeolite (LTA),[7] mordenite (MOR),[8] chabazite (SSZ-13, CHA),[9] and sodalite (SOD)[10] have been successfully prepared under solvent-free batch conditions, principally by heating mixtures of solid reactants, but combined with non-heated milling stages in some cases.

Mechanochemical synthesis techniques include ball milling (BM), thermally controlled ball milling (TCBM), twin-screw extrusion (TSE) and more recently resonant acoustic mixing (RAM). Mechanochemistry has proved to be very effective for the synthesis of other classes of microporous materials, most

[a]School of Chemistry and Chemical Engineering, Queen's University Belfast, Belfast, BT9 5AG, UK. E-mail: S.James@qub.ac.uk
[b]School of Chemistry and Chemical Engineering, Faculty of Engineering and Physical Sciences, University of Southampton, Southampton, SO17 1BJ, UK
[c]School of Chemistry, Solid-state NMR Service, Durham University, Durham, DH1 3LE, UK

notably metal–organic frameworks (MOFs), and even scaled and commercialised.[11] In those cases, often simply grinding the reactants, without heating, in the absence or near-absence of solvent, is sufficient to induce a quantitative reaction to give the crystalline MOF product.

BM in particular is often successfully applied to reactions that do not require heating. Thus, various porous materials including MOFs,[12] and covalent organic frameworks (COFs)[13] have been synthesized by BM. TCBM was reported by Uzarevic *et al.*,[14] in which an additional heater with a thermal programming system was attached to the ball mill. However, ball mills with temperature control are not widely available although notably one has now been introduced commercially.[15] Solvent-free or minimal-solvent sonochemistry and RAM have begun to be applied more recently mainly in the area of organic and MOF synthesis and are potentially scalable.[16,17] TSE is a well-established technique for materials blending and processing and has been demonstrated for the synthesis of co-crystals,[18–20] MOFs,[11,21] pigments,[22,23] and polymers.[24] Compared with the classical synthetic methods and BM based synthesis, the advantages of TSE can be summarised as: (1) greater mixing capacity; (2) better process control and (3) lower energy cost.[25] In addition, simultaneous heating is generally easily implemented in TSE equipment. Advantages over other forms of mechanochemical synthesis include continuous rather than batch operation and the ability to simultaneously perform synthesis and processing of the solid form of the product (*e.g.* into pellets).[11]

In contrast to MOFs there are relatively few reports of the purely mechanochemical synthesis of zeolites. Amongst those reports, mechanochemically-assisted solvent-free syntheses (*i.e.* where grinding is done before a heating step), has been reported to lead to products with greater crystallinity, and in shorter reaction times, than the corresponding hydrothermal syntheses.[26–29] A representative work from Nada *et al.*[30] showed that BM plays an important role in ZSM-5 solventless and template-free synthesis: ball-milling the reagents sufficiently (*i.e.*, 1400 rpm for 50 min) prior to heating in a sealed autoclave was necessary to give the desired ZSM-5 product, and insufficient (or no) milling gave to a quartz phase rather than zeolite product. Also, it should be noted that mechanochemical treatment can introduce heteroatoms into existing zeolite structures, as well as enhance their diffusion and redistribution within zeolite frameworks (example heteroatoms being Ga,[31] Zr,[32] Ce[33] *etc*).

Despite these tantalizing findings and the potential advantages of mechanochemical synthesis, to date there seems to be little if any clear evidence that zeolites can be synthesized from non-zeolite starting materials by simply grinding (*i.e.* without a subsequent heating step). Literature gives several examples where amorphous products are formed by BM or grinding rather than clearly defined crystalline zeolite products.[34] Based on the assumption that milling with concomitant heating could provide crystalline zeolite products, synthesis by TCBM and TSE are of particular interest because these methods provide grinding and heating simultaneously. To apply TSE to zeolite synthesis, there are potential challenges however, including the hardness of the materials (*e.g.* SiO_2 and Al_2O_3) which might abrade steel and reagents which can be corrosive to steel (*e.g.*, NaOH), as well as the need for relatively short reaction times because the residence time in the extruder barrel is typically up to 30 minutes, although multiple passes can potentially be done if needed.

In this work, we focus on the synthesis of sodalite (SOD), which is of interest due to its structural simplicity, lack of template requirement, and relevance to applications such as water/alcohol separation,[35] drug delivery[36] as well as H_2/CO_2 separation.[37] The SOD framework consists of interconnected cages formed by four- and six-membered rings (Scheme 1d and e). The six-membered rings define channels (~2.9 Å pore aperture)[38] that extend along the body diagonals of the cubic unit cell and intersect to form large cavities.[39] Because of its simple structure, the fact that it needs no template, and the limited success to date in solvent-free synthesis of highly crystalline material, we focused our study on this material.

Our overall aim was to elucidate the various important factors in developing an applicable, scalable, solvent-free, and ideally template-free synthetic method of zeolite synthesis, ultimately by TCBM or TSE. We have included reactants which are liquids (to enhance mass transfer and potentially provide rapid reactions) and which should have low corrosivity $Na_2SiO_3 \cdot 5H_2O$ and $Al(OAc)_2OH$.

Results and discussion

Zeolite SOD synthesis from TEOS

Initial screening involved use of $Al(OAc)_2OH$ as Al source and liquid silanes (Scheme 1a and b) tetraethylorthosilane (TEOS), phenyltriethoxysilane (PTEOS) or vinyltriethoxysilane (VTEOS) as Si source in the presence of NaOH, giving corresponding products termed TSOD, PSOD, and VSOD respectively. $Al(OAc)_2OH$ is an unusual precursor for zeolite synthesis and was chosen because has been used successfully in mechanochemical synthesis of MOFs.[40] The acetic acid by-product can potentially be helpful as an internally-generated solvent and possibly a pore template. However, in the current work it was expected to react with NaOH to form NaOAc as a by-product according to the following equation, whereas the silanes could generate EtOH as by-product:

$$3NaOH + Al(OAc)_2OH + Si(OEt)_4 \xrightarrow{180^\circ C \mid 4\ h} 2NaOAc + 1/6Na_6Al_6Si_6O_{24}\ (SOD) + 4EtOH$$

Thus, liquid silanes such as TEOS should diffuse easily through the reaction mixture and produce EtOH as by-product, a potential solvent and template. The introduction of the organic salt ($Al(OAc)_2OH$) system is particularly interesting when compared to the traditional inorganic system used in zeolite synthesis in Nada *et al.*'s work in terms of the reaction speed.[6,30]

This synthetic method was primarily used to elucidate how ball-milling pretreatment affects synthesis time and how long

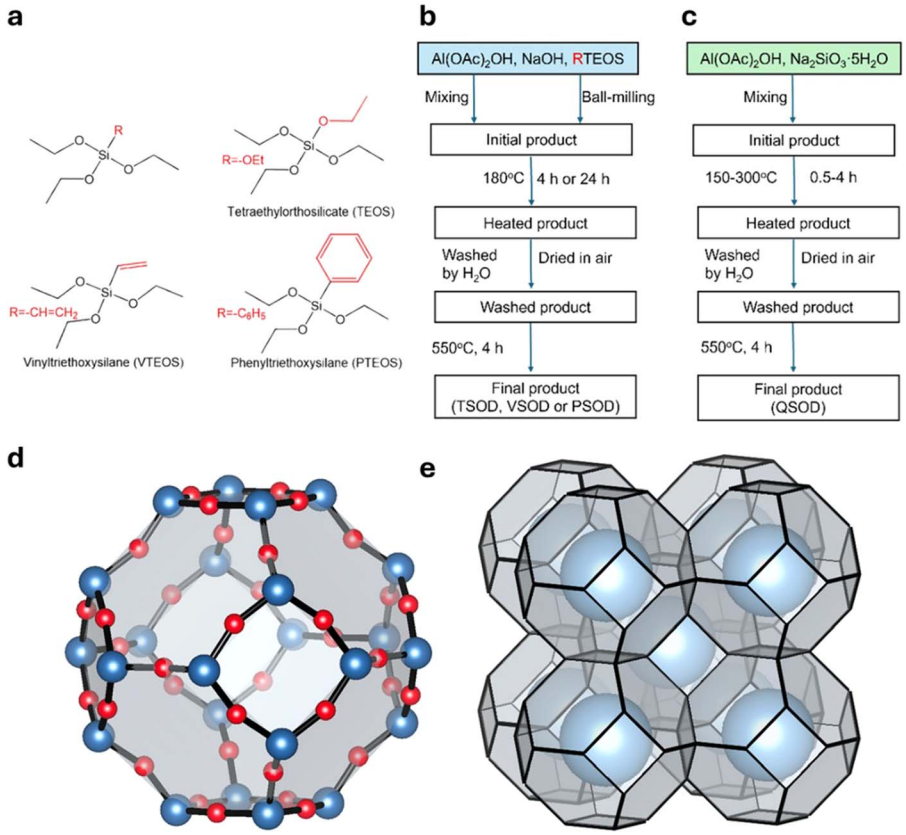

Scheme 1 (a) Structures of tetraethyl silicate (TEOS), vinyltriethoxysilane (VTEOS) and phenyltriethoxysilane (PTEOS), (b) procedure for the synthesis of zeolite SOD from alkoxysilanes, and (c) procedure for the synthesis of zeolite SOD from $Na_2SiO_3 \cdot 5H_2O$, (d) structure of one sodalite cage (red = oxygen, blue = Si or Al) and (e) cubic arrangement of 8 sodalite cages in the zeolite structure.

the reaction takes to obtain moderately crystalline (*i.e.* crystallinity > 50%) SOD. The level of crystallinity was determined by the ratio of the sum of the areas under the diffraction peaks corresponding to the SOD crystalline phase to the total area under the diffraction curve within the specified range for SOD.

Two initial mixing/milling methods were employed: either manual mixing with a spatula for 3–5 minutes or ball milling at 23.3 Hz for 50 minutes (the same frequency as used by Nada *et al.*[30]), as illustrated in the Scheme 1b.

Using TEOS as the silica source, from the PXRD data shown in Fig. 1a, it is clear that simple manual mixing, or ball milling TEOS, $Al(OAc)_2OH$ and NaOH at 23.3 Hz for 50 minutes leads to a mixture of an amorphous product phase and crystalline NaOAc as by-product (ICDC code: JCPD#00-01-0050). The ball-milled mixture yields a more crystalline NaOAc by-product phase compared with simply mixing, as is evident from the sharper and more intense reflections. However, neither mixing method produced crystalline SOD, and after washing to remove NaOAc only amorphous material remained. However, taking the manually mixed reactants and heating them at 180 °C for 4 h in a sealed Teflon-lined stainless-steel autoclave did convert it to crystalline SOD together with crystalline NaOAc as revealed by PXRD. A water washing step removed the NaOAc by-product to leave the SOD product according to PXRD.

Combining initial reagent mixing with a spatula and subsequent heating at 180 °C, it was found that extending the reaction time to 24 hours increased crystallinity only slightly from 31% to 35% at 1.5 g scale, as shown in Fig. 1c. However, at larger scale (7.5 g) the longer reaction time increased the crystallinity from 49% to 74%. Interestingly, the amorphous product from the ball milling procedure required longer heating (48 h) to give a crystalline product than did the amorphous phase obtained by simple mixing (which required only 24 h heating to give crystalline SOD product). This suggests that too much mechanical treatment prior to heating can actually be disadvantageous. With these optimizations, the sample that exhibited the greatest crystallinity (hand mixing, 24 hours heating, 7.5 g scale) was designated as "TSOD" and used for the further characterization.

TSOD gave a PXRD pattern that fitted well with the simulated pattern for SOD (Fig. 1a, see SI for the simulation procedure) with no additional peaks identifiable.

Analysis by ^{27}Al MAS NMR at various stages of the synthesis process showed the change in Al environment (Fig. 1b). According to literature,[41] signals due to tetrahedral AlO_4 centres should occur from 55–80 ppm and those for octahedral AlO_6 centres from 0 to 16 ppm. The starting material $Al(OAc)_2OH$ showed a broad feature due to quadrupolar interaction from −15 to −49 ppm suggesting octahedral Al. Interestingly,

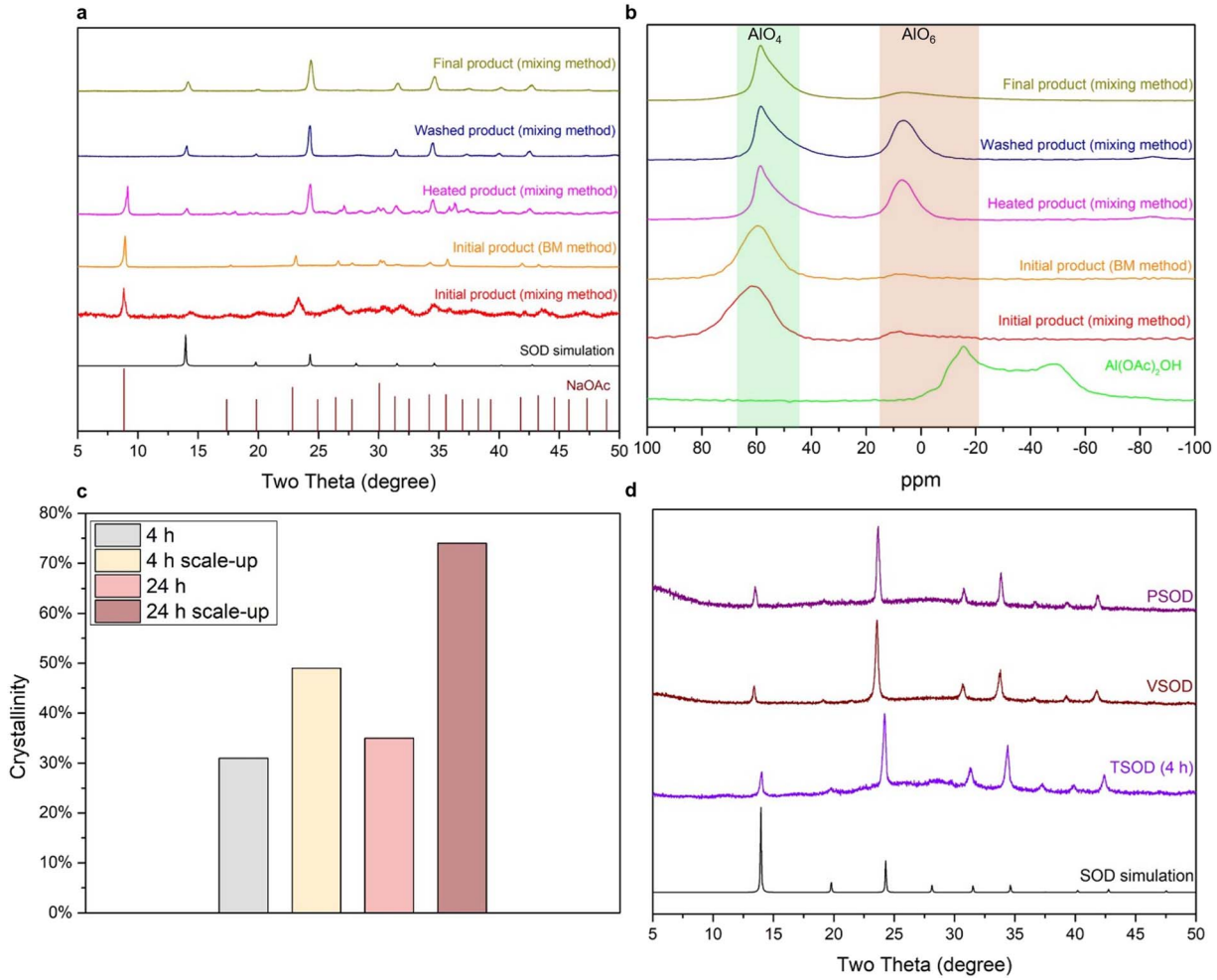

Fig. 1 (a) PXRD pattern of each step: reactant mixture, after heated, after washed, and after calcined. Note that both initial product by BM method (orange) and mixing method (red) showed main phase is NaOAc (ICDD database code: JCPD#00-01-0050); (b) ^{27}Al MAS NMR of the starting material $Al(OAc)_2OH$, reactant mixture, after heated, after washed and after calcined; (c) crystallinity of the synthesized TSOD across different starting material scale and reaction time; (d) PXRD pattern of synthesized TSOD (4 h), VSOD and PSOD.

a quantitative change in Al environmental was observed even after simple hand mixing of the reagents. In particular, whilst a small peak suggesting disordered AlO_6 centres was retained it is clearly distinct from the starting material due to its different line shape (7.1 ppm, FWHM = 1025 Hz). Importantly, a more intense resonance centred at 62.3 ppm suggesting a disordered AlO_4 environment is present (FWHM = 1947 Hz). The milled sample gave a similar spectrum with a slightly sharper AlO_6 peak (FWHM = 1602 Hz). After heating, the AlO_6 signal (7.0 ppm, FWHM = 1074 Hz) increased in intensity relative to the unheated sample. Also, the AlO_4 peak became less broad (56.2 ppm, FWHM = 1283 Hz) consistent with formation of a more crystalline product, most likely the SOD framework as seen in the PXRD data. After washing to remove by-products, the TSOD product gave a spectrum which was largely unchanged. After calcination at 550 °C for 4 h, the TSOD sample shows an AlO_4 peak (55.5 ppm, FWHM = 1281 Hz) and an AlO_6 peak with much-decreased relative intensity (5.8 ppm, FWHM = 2333 Hz). The ^{27}Al multiple-quantum magic angle spinning (MQMAS) NMR then further verified the existence of the AlO_4 and AlO_6 environment (Fig. S4b) in TSOD.

Overall, the PXRD and ^{27}Al MAS NMR results suggest that the hand-mixing or ball-milling processes each induce a quantitative reaction between the starting materials but only serve to provide an amorphous Al–O–Si network with relatively disordered AlO_4 centres. Formation of a crystalline product with the SOD structure requires subsequent heating. This is consistent with the high enthalpies of the Si–O and Al–O bonds which must be broken and reformed to give a crystalline product. It also contrasts with many mechanochemical MOF syntheses which do not require heating and which are more generally based on more labile M–L bonds.

FT-IR analysis of TSOD (see Fig. S1) showed a characteristic band at 980–997 cm^{-1}, due to symmetrical T–O–T (T = Si, Al) vibration but, interestingly, also carboxylate bands at 1586 cm^{-1} and 1420 cm^{-1}. Reports of acetate impregnation of zeolite SOD are rare.[42] However, these IR data are similar to those reported in Sieger *et al.*'s study (1594 and 1420 cm^{-1}),[43] where NaOAc was used in the solvothermal synthesis to give acetate-impregnated

SOD phase of formula $[Al_3Si_3O_{12}]_2[Na_4OAc]_2$. In that work, a range of techniques including single-crystal X-ray diffraction supported the incorporation of acetate group into the zeolite pores. Within each sodalite cavity there is a tetrahedral arrangement of Na^+ ions which are closely associated with the O atoms of the framework, with a crystallographically disordered acetate anion at the centre of the Na_4 tetrahedron.

TGA of TSOD suggested that the acetate group was incorporated into the zeolite structure rather than being present as an impurity. In particular, under N_2 atmosphere, the TGA curve of the starting material $Al(OAc)_2OH$ (Fig. S2) shows decomposition to Al_2O_3 occurring in three steps (percentage weight losses of 7.4, 50.4 and 9.3% at <63, 63–383 and >383 °C respectively, with a total weight loss of 67.2%, which is close to the calculated value of 68.6%) in agreement with literature.[44] The DTG curve shows the most rapid weight loss (1%/°C) centred at 288 °C. It can be noted that in Sato *et al.*'s study[44] a low intensity $\nu_{C=O}$ IR signal was observed even up to 800 °C, possibly indicating minor residual acetate. In contrast, the TGA curve of TSOD (Fig. S3) shows weight-loss occurring in 5 steps (2.7, 1.3, 3.0, 1.8 and 3.9% at 30–150, 150–377, 377–548, 548–712 and >718 °C respectively, total weight-loss 13.7%) with the DTG curve showing fastest weight-loss (0.03%/°C) occurring at 480 and 803 °C. We ascribe these processes to the loss of water and acetate. Crucially, the TGA features for $Al(OAc)_2OH$ are not seen in the TSOD product, and we therefore conclude that the acetate is indeed incorporated within the zeolite structure. TGA data for each weight-loss step are summarized in Table S3.

As shown in Fig. S5a, $Al(OAc)_2OH$ shows two carbon environments in its solid state NMR spectrum – the acetate COO peak at 179.8 ppm, and the acetate methyl peak at 25.3 ppm. The ^{13}C MAS NMR shown in Fig. S5b reveals that the spectra obtained for the washed TSOD sample similarly features two ^{13}C signals, slightly shifted to 180.8 ppm and 27.3 ppm. The calcination does not lead to significant changes in chemical shift (180.5 and 27.3 ppm) but does lead to a decrease in the peak intensity, which can be ascribed to partial loss of the acetate group. Moreover, from the elemental analysis shown in Table S4, there is an excess of Al (3.72 wt%) and C (3.57 wt%) in the TSOD sample compared to the SOD formula ($Na_6Al_6Si_6O_{24}$), which suggests a chemical formula of $[Al_3Si_3O_{12}]_2[Na_2Al(OAc)OH]_2$.

The N_2 isotherm shown in Fig. S6a indicates that as-synthesized TSOD exhibits a Type II isotherm, which is characteristic of materials with low porosity. This observation is primarily attributed to the small window size of the SOD cages, which restricts N_2 access to the internal pore structure. The N_2-BET surface area was determined to be 24.2 $m^2\ g^{-1}$, which is in the range reported in literature (5.5–42.9 $m^2\ g^{-1}$).[35,45] These are low values amongst microporous materials consistent with the small pore windows allowing little N_2 absorption. SEM images reveal that the particle size ranges from 40 to 1500 nm (Fig. S7a).

Organo-zeolite SOD synthesis from organosilanes (VTEOS or PTEOS)

We also investigated whether these synthetic conditions could be generalised to solvent-free synthesis of organo-zeolites by using vinyltriethoxysilane (VTEOS) or phenyltriethoxysilane (PTEOS) in place of TEOS. Organo-zeolites have not previously been reported *via* solvent-free synthesis using VTEOS or PTEOS as the sole Si source.[46] Instead, they are typically prepared *via* solvothermal methods,[47,48] or through solvent-free synthesis using a combination of organosilane and SiO_2.[46] In our study, 4 h reaction time was used, and conditions were not optimised for these products.

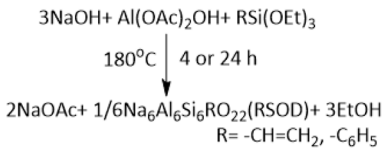

The products obtained from VTEOS and PTEOS are referred to as VSOD and PSOD, respectively. As shown in Fig. 1d, they give PXRD patterns consistent with the formation of SOD frameworks. The crystallinity calculated from the PXRD data was greater for VSOD (44%) than for TSOD after 4 h reaction time (31%), whereas the crystallinity of PSOD was similar (30%). IR spectroscopy showed the expected bands attributable to the vinyl and phenyl groups as well bands attributable to acetate groups suggesting that these products were acetate-impregnated as for TSOD (Fig. S1). Further characterisation of VSOD was done. The ^{27}Al MAS NMR spectrum was similar to that of TSOD, albeit with differences in peak breadth, showing a major peak due to both AlO_4 (57.3 ppm) and a minor AlO_6 peak (4.2 ppm) (Fig. S4a). The ^{13}C MAS NMR spectrum shows peaks attributable to the acetate COO group (180.9 ppm), the acetate methyl group (27.3 ppm) and the two vinyl carbons at 134.6 ppm which could not be individually resolved. These chemical shifts are reasonable given that the solution ^{13}C NMR spectrum of VTEOS (in $CDCl_3$) gives vinyl peaks at 137.2 and 129.4 ppm, with the ethoxy group at 58.7 and 18.4 ppm (Fig. S5). Overall, these results support the expected incorporation of the vinyl group attached to Si into the SOD structure.

Interestingly, VSOD gave a Type IV isotherm (Fig. S6b) indicating that the sample was both microporous and mesoporous, with an apparent surface area of 181.2 $m^2\ g^{-1}$, significantly greater than that of TSOD, possibly due to the greater proportion of amorphous phase in the sample. Textural differences were also seen by SEM which showed particle size ranging from 500 to 3000 nm, greater than for TSOD (40–1500 nm) (Fig. S7b). Based on both the N_2 adsorption isotherm and SEM observations, the isotherm behaviour likely reflects a combination of inter-crystalline (textural) porosity and some degree of mesoporosity, although their relative contributions cannot be unambiguously distinguished from the present data.[48]

As summarised in Table S5, comparing with the reported literature,[35,45,49–51] use of TEOS as the silicon source allows the SOD synthesis to be shortened to 4 h and the crystallinity could be up to 74% depending on the reaction conditions. Moreover, SOD synthesis with by organosilanes provided more SOD derivatives with different organic functional groups, which provides a plausible synthetic method for surface modification for example.

Electron diffraction structure determinations

To further verify that TSOD and VSOD have similar structures to the reported SOD structure, 3D electron diffraction experiments were conducted. The measurements were performed at 175(5) K, attempting to reduce thermal motion and effects of the high vacuum conditions on the materials and their potential guest species. For each material, data were collected from several individual crystals, and subsequently merged to produce a dataset for crystal structure analysis. Structures for both materials were indexed in a cubic unit cell with $a = 9.0311(7)$ for TSOD and $a = 9.0718(9)$ for VSOD. Both structures were solved and refined in space group $P\bar{4}3n$ allowing separate T sites for aluminium and silicon.[43,52] Residual electrostatic potential maxima were assigned to sodium cations, balancing the negatively charged aluminosilicate framework. In the case of TSOD, two partially occupied sites for sodium cations were identified, whereas for VSOD three such sites were included. The total amount of sodium is identical for both structures and matches the aluminium content. Neither structure showed convincing crystallographic evidence of ordered acetate (or vinyl groups in the case of VSOD), although we note the slightly larger unit cell for VSOD which may correspond to the accommodation of vinyl groups. Some unmodeled residual electrostatic potential indicates the possibility for disordered, unaccounted-for guest species such as the respective organic groups or water. However, no distinct feature could be discerned. It is also possible that some of the positions assigned to sodium may be occupied by any of these guest species, but from the obtained data such analysis was deemed inconclusive. Further information about the 3DED experiments and the obtained crystal structures can be found in Tables S1 and S2. The obtained crystal structures for TSOD and VSOD are shown in Fig. 2 and S8a, b.

Zeolite SOD synthesis from $Na_2SiO_3 \cdot 5H_2O$

To further minimize the reaction time, temperature and corrosivity, we then investigated alternative starting materials to those used above, including Si source (*e.g.*, SiO_2, TEOS), Al source (*e.g.*, $Al(OH)_3$, $Al(OAc)_2OH$ and $Al(iPrO)_3$) and base (NaOH, $NaHCO_3$) in various combinations. Most notably, we found that use of $Na_2SiO_3 \cdot 5H_2O$ as Si source enabled us to avoid the use of potentially corrosive base NaOH. SOD could thereby be obtained after simply hand-mixing the solid starting materials $Al(OAc)_2OH$ and $Na_2SiO_3 \cdot 5H_2O$ for up to 5 minutes and heating at 300 °C for 4 h in a closed vessel. Synthesis was done at 2 g scale (product denoted as QSOD) and 20 g scale (product referred to QSOD-scale up). The products and by-product were characterized using PXRD analysis, with the characterization procedure detailed in Fig. 3a.

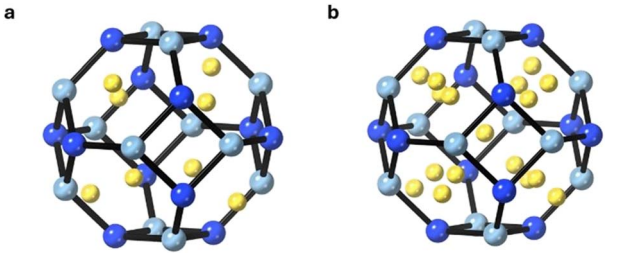

Fig. 2 Unit cells of TSOD (a) and VSOD (b) obtained by electron diffraction structure determination (light blue = Si, dark blue = Al, yellow = Na). Na is distributed over two partially occupied sites in TSOD and three sites for VSOD.

The PXRD patterns for unpurified product (Fig. S9) clearly show the expected pattern for SOD and suggest that the main by-product is $NaOAc \cdot 3H_2O$ (ICDD code: JCPD# 00-028-1030). Due to overlapping of PXRD peaks, multiple by-products may be present. A possible combination includes $Na_2Si_2O_5$ (ICDD code: JCPD# 00-053-1234) and NaOH (ICDD code: JCPD# 97-000-5458). A tentative equation for the reaction based on these observations is therefore:

$$3Na_2SiO_3 \cdot 5H_2O + Al(OAc)_2OH \xrightarrow[100\text{-}300^{\circ}C \mid 0.5\text{-}4\ h]{} 2NaOAc \cdot 3H_2O + 1/6Na_6Al_6Si_6O_{24}\ (SOD) + Na_2Si_2O_5 + NaOH \cdot 4H_2O + 5H_2O$$

The effects of varying reaction time and temperature were studied using an autoclave and preheated oven. The crystallinity of the product was taken as a measure of the conversion to SOD and the results are summarised in Fig. 3c. At 100 °C, the formation of SOD was only observed after 4 h, whereas as at 300 °C significant conversion had occurred even after only 0.5 h. Fig. 3d shows that preheating the autoclave enabled reasonable crystallinity (*i.e.*, ~60%) to be achieved after only 0.5 h even at 150 °C. While for a 0.25 h reaction, across the test range, 180 °C was required to give a crystalline SOD product.

Optimised synthesis conditions for QSOD provided material with a good level of crystallinity (82%). All PXRD peaks matched well with the simulated pattern, except for the absence of the (220) peak at 28.5°. This could be attributed to structural disorder causing peak broadening or intensity loss. All PXRD peaks fitted well to the simulated pattern albeit with the (220) peak at 28.5° absent. Interestingly, use of these conditions for QSOD-scaleup gave still higher crystallinity (94%) with 92% isolated yield after washing to remove byproducts and calcination (Fig. 3b). IR spectra (Fig. S10) were similar to that of TSOD including bands at 1592 and 1419 cm^{-1} assigned to the –O–C=O asymmetric and symmetric stretching of included acetate, the presence of which was also supported by ^{13}C MAS NMR spectrum (Fig. 3e) (singlets at 27.3 ppm and 180.6 ppm). The ^{27}Al MAS NMR spectrum of QSOD (Fig. 3f) shows only a AlO_4 environment (59.0 ppm), indicating that the acetate is not bound to Al. Based on the elemental analysis (Table S4), QSOD-scaleup has composition $Si_{4.5}$ $Al_{4.1}$ $C_{3.1}$ $H_{4.2}$, consistent with the chemical formula $[Al_3Si_3O_{12}]_2[Na_4OAc]_2$ as in the work of Sieger *et al.*[43]

The N_2 isotherm shown in Fig. S11 indicates that as-synthesized QSOD has low porosity (Type II isotherm) with an apparent BET surface area of 42.4 $m^2\ g^{-1}$, while QSOD-scale up has a lower surface area of 10.5 $m^2\ g^{-1}$. Whilst low for microporous materials due to the restricted window size of SOD, these values fall within the range reported in the literature (5.5–42.9

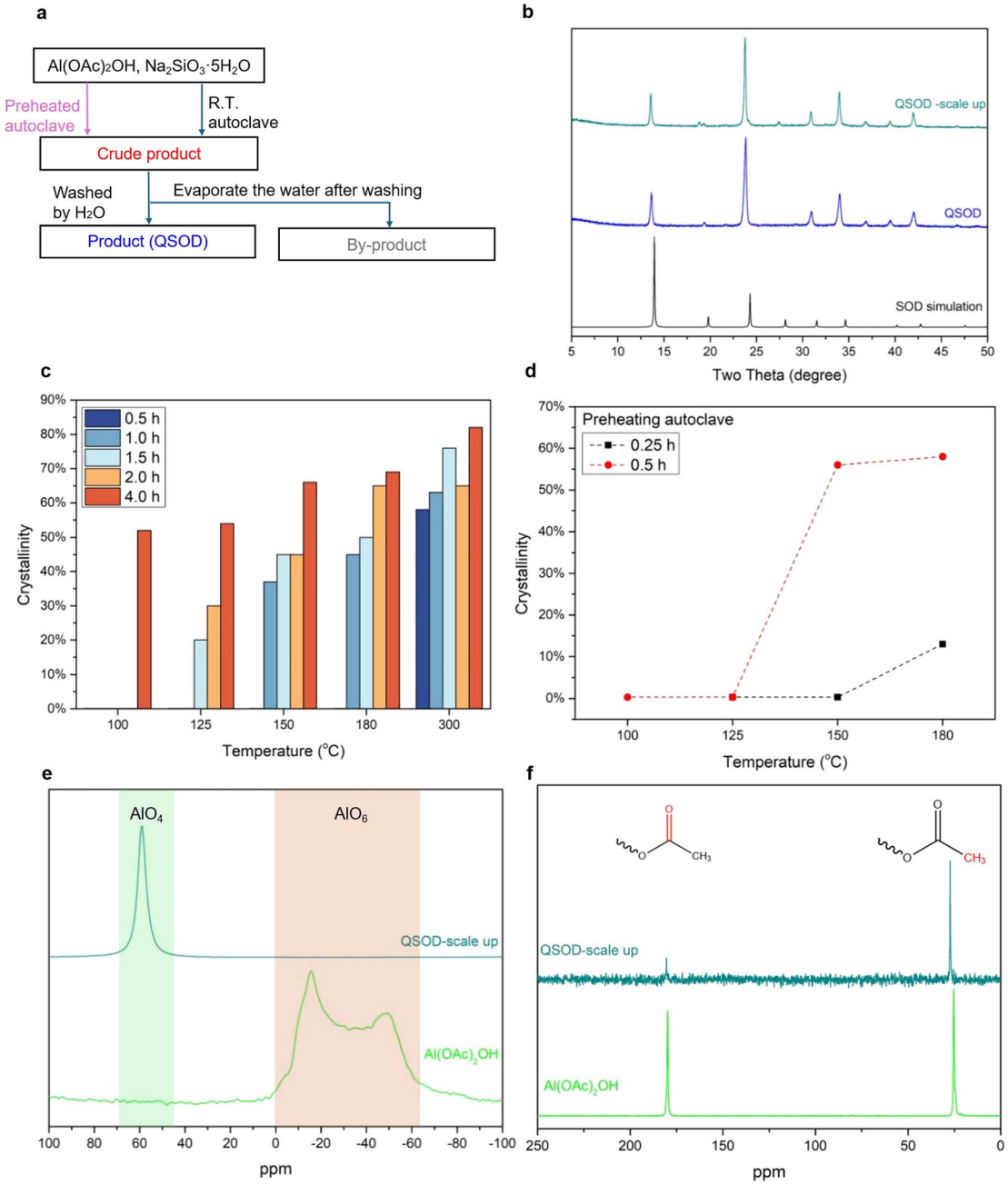

Fig. 3 (a) Scheme of by-product characterization and preheating effects investigation; (b) PXRD pattern of the QSOD, QSOD-scaleup and the SOD simulation pattern; (c) PXRD-calculated crystallinity of synthesized SOD across different temperature and reaction time; (d) PXRD-calculated crystallinity of reaction performed in pre-heated autoclave for 0.25 h and 0.5 h. Note: refer to the SI for the crystallinity calculation and the standard PXRD pattern simulation method; (e) ^{27}Al MAS NMR of as synthesized QSOD-scale up and the starting material $Al(OAc)_2OH$; and (f) ^{13}C MAS NMR of the as synthesized QSOD-scale up and the starting material $Al(OAc)_2OH$.

$m^2\ g^{-1}$) for SOD.[35,45] SEM images reveal that the particle size is centred around 150 nm for QSOD and 100–200 nm for QSOD-scaleup (Fig. S12).

Exploring potential for larger-scale zeolite synthesis by TCBM and TSE

To further assess the possibility to apply these latter reagents in TCBM and TSE, in terms of their corrosivity and the degree of wear on steel media, heating and milling tests were performed using stainless-steel components. As shown in Fig. S13, a new stainless-steel (416L) milling ball and a new screw element were placed in a sealed Teflon-lined stainless-steel autoclave with the starting materials and heated at 100–300 °C for 4 h. Little or no corrosion was visible upon heating at 100–150 °C, although the milling ball did show some corrosion after heating to 180 °C, and ultimately became black after heating at 300 °C. As shown in Fig. S14, after ball-milling at 23.3 Hz for 50 min, neither the

milling jar nor ball showed any evidence of corrosion. There for it may be possible to conduct this synthesis under TCBM or TSE conditions at 150 °C at least over short reaction times (*e.g.*, 0.5 h) without corroding the contacting media.

An initial attempt was made to conduct zeolite SOD synthesis by TSE using $Al(OAc)_2OH$ and $Na_2SiO_3 \cdot 5H_2O$ at 150 °C and 55 rpm. However, unexpectedly the reaction mixture rapidly formed an immobile gel causing the torque to increase rapidly and torquing out of the extruder motor within 10 minutes. PXRD showed that the crude product in the extruder barrel contained crystalline sodium acetate indicating that at least partial reaction had occurred. However, after washing to remove this, only an amorphous phase remained suggesting that there was insufficient heating/time to generate the crystalline zeolite structure.

The formation of a hard, immobile gel was surprising given that this behaviour had not been observed during milling or heating. We relate this difference to rapid dehydration of $NaSiO_3 \cdot 5H_2O$, which can occur in the extruder since it is an open system, in contrast to the closed jars used in the above experiments. Therefore, in order to achieve zeolite synthesis by TSE, it is likely that an alternative reaction system should be found which can operate in an open system. Further work in this line will be reported in due course.

Beyond the specific system studied here, these findings underscore a broader challenge in translating solid-state and solvothermal syntheses to continuous processing platforms such as twin-screw extrusion. In particular, the balance between hydration, phase evolution, and mass transport appears to be highly sensitive to whether the reaction is conducted in a closed or open environment. This suggests that successful implementation of TSE for zeolite synthesis may require not only adaptation of existing chemistries but, more fundamentally, the development of reaction systems intrinsically compatible with continuous, open processing conditions. Approaches such as the use of more stable hydrated precursors, *in situ* water management strategies, or alternative structure-directing routes could prove essential. More generally, these considerations highlight the need to rethink reaction design principles when moving from batch to continuous mechanochemical processes.

Conclusions

To sum up the most salient point for the mechanochemical solvent-free synthesis of zeolites: grinding seems to be less critical than heating. Even simple hand-mixing for a few minutes can in some cases give a quantitative reaction between Si and Al-containing reactants, but the products formed by simply mixing/grinding are invariably amorphous. In all cases, heating was needed to crystallise the product into the zeolite structure. The reason for this difference with mechanochemical MOF synthesis (which often only requires grinding with no heating) is likely due to the greater Si–O and Al–O bond strengths in zeolites which make the kinetic amorphous products less labile and their crystallisation into the zeolite structure more energy-intensive, *i.e.* requiring heating. These considerations point to TSE which provides simultaneous mixing and heating, as a promising approach to solventless zeolite manufacturing (combined with its inherent advantages of continuous nature, potential to combine synthesis with processing *etc.*). Further, the above work shows that reaction systems can be found which are non-corrosive to steel and which only require a few minutes heating, consistent with the typical residence times in TSE. However, a final challenge highlighted identified here is that TSE is normally an open system. This means that the requirement for heating can cause volatiles such as water (by-product) to be lost, resulting in partially-reacted immobile solid phases. Therefore, reaction conditions or engineering need to be put in place which overcome the loss of volatiles, or reaction chemistry identified for which the loss of volatiles is not an issue. We will report further on possible solutions to this challenge in due course.

Conflicts of interest

There are no conflicts to declare.

Data availability

The data supporting this article have been included as part of the supplementary information (SI). Supplementary information is available. See DOI: https://doi.org/10.1039/d6mr00009f.

Deposition numbers 2432426 and 2432427 contain the supplementary crystallographic data for this paper. These data can be obtained free of charge *via* the joint Cambridge Crystallographic Data Centre (CCDC) and Fachinformationszentrum Karlsruhe Access Structures service.[53a,b]

The 3D ED raw data have been deposited with the 3D ED Zenodo community and can be accessed at https://doi.org/10.5281/zenodo.18348337.

Acknowledgements

The authors gratefully acknowledge the financial support provided by the China Scholarship Council (CSC) under Grant No. 202106880009. D. N. R. and S. J. C. thank the EPSRC for funding (EP/X014444/1 and EP/X014606/1, A National Electron Diffraction Facility for Nanomaterial Structural Studies). We thank Ms Anna Clarke for generating zeolite Fig. 1d and e.

Notes and references

1 S. M. Auerbach, K. A. Carrado and P. K. Dutta, *Handbook of Zeolite Science and Technology*, CRC Press, 2003.
2 A. Kornas, J. E. Olszówka, P. Klein and V. Pashkova, *Catalysts*, 2021, **11**, DOI: 10.3390/catal110202406.
3 X. Meng and F.-S. Xiao, *Chem. Rev.*, 2014, **114**, 1521–1543.
4 D. N. Rainer and R. E. Morris, *Dalton Trans.*, 2021, **50**, 8995–9009.
5 Q. Wu, X. Meng, X. Gao and F.-S. Xiao, *Acc. Chem. Res.*, 2018, **51**, 1396–1403.
6 M. H. Nada, E. G. Gillan and S. C. Larsen, *Microporous Mesoporous Mater.*, 2019, **276**, 23–28.

7 Y. Xiao, N. Sheng, Y. Chu, Y. Wang, Q. Wu, X. Liu, F. Deng, X. Meng and Z. Feng, *Microporous Mesoporous Mater.*, 2017, **237**, 201–209.
8 W. Gao, C. C. Amoo, G. Zhang, M. Javed, B. Mazonde, C. Lu, R. Yang, C. Xing and N. Tsubaki, *Microporous Mesoporous Mater.*, 2019, **280**, 187–194.
9 V. Pashkova, K. Mlekodaj, P. Klein, L. Brabec, R. Zouzelka, J. Rathousky, V. Tokarova and J. Dedecek, *Chem.–Eur. J.*, 2019, **25**, 12068–12073.
10 L. Ren, Q. Wu, C. Yang, L. Zhu, C. Li, P. Zhang, H. Zhang, X. Meng and F.-S. Xiao, *J. Am. Chem. Soc.*, 2012, **134**, 15173–15176.
11 D. Crawford, J. Casaban, R. Haydon, N. Giri, T. McNally and S. L. James, *Chem. Sci.*, 2015, **6**, 1645–1649.
12 N. K. Singh, M. Hardi and V. P. Balema, *Chem. Commun.*, 2013, **49**, 972–974.
13 D. Huang, X. Yan, M. Yan, G. Zeng, C. Zhou, J. Wan, M. Cheng and W. Xue, *ACS Appl. Mater. Interfaces*, 2018, **10**, 21035–21055.
14 N. Cindro, M. Tireli, B. Karadeniz, T. Mrla and K. Užarević, *ACS Sustain. Chem. Eng.*, 2019, **7**, 16301–16309.
15 https://www.retsch.com/products/milling/ball-mills/mm-500-control/.
16 Y. Luo, D. Chen, F. Wei and Z. Liang, *ChemistrySelect*, 2018, **3**, 11435–11440.
17 H. M. Titi, J.-L. Do, A. J. Howarth, K. Nagapudi and T. Friščić, *Chem. Sci.*, 2020, **11**, 7578–7584.
18 R. S. Dhumal, A. L. Kelly, P. York, P. D. Coates and A. Paradkar, *Pharm. Res.*, 2010, **27**, 2725–2733.
19 C. Medina, D. Daurio, K. Nagapudi and F. Alvarez-Nunez, *J. Pharm. Sci.*, 2010, **99**, 1693–1696.
20 D. Daurio, K. Nagapudi, L. Li, P. Quan and F.-A. Nunez, *Faraday Discuss.*, 2014, **170**, 235–249.
21 B. Karadeniz, A. J. Howarth, T. Stolar, T. Islamoglu, I. Dejanović, M. Tireli, M. C. Wasson, S.-Y. Moon, O. K. Farha, T. Friščić and K. Užarević, *ACS Sustain. Chem. Eng.*, 2018, **6**, 15841–15849.
22 Q. Cao, D. E. Crawford, C. Shi and S. L. James, *Angew. Chem.*, 2020, **132**, 4508–4513.
23 D. Thetford, A. P. Chorlton and J. Hardman, *Dyes Pigm.*, 2003, **59**, 185–191.
24 A. Rubin Pedrazzo, F. Trotta, G. Hoti, F. Cesano and M. Zanetti, *Environ. Sci. Pollut. Res.*, 2022, **29**, 251–263.
25 U. Nandi, V. Trivedi, S. A. Ross and D. Douroumis, *Pharmaceutics*, 2021, **13**, 624.
26 S. Zhao, H. Li, W. Zhang, B. Wang, X. Yang, Y. Peng, Y. Zhang and Z. Li, *Catalysts*, 2022, **12**, 301.
27 Y. Mu, Y. Zhang, J. Fan and C. Guo, *Ultrason. Sonochem.*, 2017, **38**, 430–436.
28 R. Karimi, B. Bayati, N. Charchi Aghdam, M. Ejtemaee and A. A. Babaluo, *Powder Technol.*, 2012, **229**, 229–236.
29 Z. Wu, S. Goel, M. Choi and E. Iglesia, *J. Catal.*, 2014, **311**, 458–468.
30 M. H. Nada, S. C. Larsen and E. G. Gillan, *Nanoscale Adv.*, 2019, **1**, 3918–3928.
31 M. Yabushita, M. Yoshida, F. Muto, M. Horie, Y. Kunitake, T. Nishitoba, S. Maki, K. Kanie, T. Yokoi and A. Muramatsu, *Mol. Catal.*, 2019, **478**, 110579.
32 H. Zhang, S. Jaenicke, K. Okumura, H.-R. Tan and G.-K. Chuah, *J. Catal.*, 2024, **431**, 115398.
33 G. Majano, L. Borchardt, S. Mitchell, V. Valtchev and J. Pérez-Ramírez, *Microporous Mesoporous Mater.*, 2014, **194**, 106–114.
34 V. Y. Prokof'ev, N. E. Gordina, A. B. Zhidkova and A. M. Efremov, *J. Mater. Sci.*, 2012, **47**, 5385–5392.
35 S. Khajavi, J. C. Jansen and F. Kapteijn, *J. Membr. Sci.*, 2009, **326**, 153–160.
36 S. Rahmani, S. N. Azizi and N. Asemi, *Int. Curr. Pharm. J.*, 2016, **5**, 55–58.
37 M. S. Nabavi, T. Mohammadi and M. Kazemimoghadam, *Ceram. Int.*, 2014, **40**, 5889–5896.
38 G. V. Shanbhag, M. Choi, J. Kim and R. Ryoo, *J. Catal.*, 2009, **264**, 88–92.
39 M. Arockiaraj, J. Clement, D. Paul and K. Balasubramanian, *J. Mol. Struct.*, 2021, **1223**, 128766.
40 F. E. Salvador, Z. Tegudeer, H. Locke and W.-Y. Gao, *Dalton Trans.*, 2024, **53**, 4406–4411.
41 P. S. Singh, M. Trigg, I. Burgar and T. Bastow, *Mater. Sci. Eng., A*, 2005, **396**, 392–402.
42 G. Engelhardt, J. Felsche and P. Sieger, *J. Am. Chem. Soc.*, 1992, **114**, 1173–1182.
43 P. Sieger, A. M. Schneider, M. Wiebcke, P. Behrens, J. Felsche and G. Engelhardt, *Chem. Mater.*, 1995, **7**, 163–170.
44 T. Sato, S. Ikoma and F. Ozawa, *Thermochim. Acta*, 1984, **75**, 129–137.
45 X. Jiang, Y. Zhang and Y. Zhang, *React. Kinet., Mech. Catal.*, 2019, **127**, 489–504.
46 D. I. Petkowicz, S. Canal, P. H. Finger, M. L. Mignoni and J. H. Z. dos Santos, *Microporous Mesoporous Mater.*, 2017, **241**, 98–106.
47 B.-Z. Zhan, M. A. White and M. Lumsden, *Langmuir*, 2003, **19**, 4205–4210.
48 A. S. Maria Chong, X. S. Zhao, A. T. Kustedjo and S. Z. Qiao, *Microporous Mesoporous Mater.*, 2004, **72**, 33–42.
49 C. L. Eden and M. O. Daramola, *Mater. Today: Proc.*, 2021, **38**, 522–527.
50 W. Franus, M. Wdowin and M. Franus, *Environ. Monit. Assess.*, 2014, **186**, 5721–5729.
51 S. Zeng, R. Wang, A. Li, W. Huang, Z. Zhang and S. Qiu, *CrystEngComm*, 2016, **18**, 6779–6783.
52 J. Löns and H. Schulz, *Acta Crystallogr.*, 1967, **23**, 434–436.
53 (*a*) CCDC 2432426: Experimental Crystal Structure Determination, 2026, DOI: 10.25505/fiz.icsd.cc2mn4ct; (*b*) CCDC 2432427: Experimental Crystal Structure Determination, 2026, DOI: 10.25505/fiz.icsd.cc2mn4dv.